TAO, Vol.5, No.4, 557-571, December 1994

Oceanic Phenomena Northeast of Taiwan From Almaz SAR Image

CHO-TENG LIU[1], LEONID MITNIK[2], MING-KUANG HSU[2] and YIH YANG[1]

(Manuscript received 23 February 1994, in final form 28 August 1994)

ABSTRACT

The first analysis of a Synthetic Aperture Radar (SAR) image over Taiwan area is presented. This image was obtained from the Russian Almaz satellite of pass 7519. The brightness of the SAR images represents the backscattering cross section of the sea surface or the roughness of the sea surface that responds dynamically to the surface wind, the surfactant concentration and the divergence of surface current. Because SAR uses microwave as a working frequency, it can provide an un-fragmented image of the sea surface with the least interference from the cloud or weather system. In this study, weather maps, wave analysis maps, ship data, satellite thermal images and bathymetric charts were used to interpret the brightness variations of the SAR image northeast of Taiwan, and a wealth of oceanic features -- slicks, surface waves, packets of internal waves, current, bottom topography, vortices, ships and ship wakes were found. These features should be further validated with shipborne measurements, satellite IR data, and SAR images from other satellites, like the first European Space Agency remote sensing satellite, the ERS-1.

(Key words: SAR, Taiwan, Oceanography, Almaz)

1. INTRODUCTION

The region northeast of Taiwan is a region of special interest to local oceanographers. Oceanographic research projects in Taiwan have concentrated on Kuroshio-related studies since 1989, such as the Kuroshio Edge Exchange Processes (KEEP) and the World Ocean Circulation Experiment. Such efforts resulted in a better understanding of the interaction between the Kuroshio and the East China Sea water. The hydrophysical characteristics and space-time variability of the upwelling northeast of Taiwan and the Kuroshio were investigated by contact methods during sea expeditions (Liu *et al.*, 1992b), by analysis of NOAA

[1] Institute of Oceanography, National Taiwan University, Taipei, Taiwan, R.O.C.

[2] Department of Oceanography, National Taiwan Ocean University, Keelung, Taiwan, R.O.C.

thermal imageries (Lin *et al.*, 1992) and by comparison with model calculations (Hsueh *et al.*, 1992; Liu *et al.*, 1992a).

The Kuroshio edge exchange processes and the upwelling phenomena should be governed by the interaction among forces or factors of long time scale: the Kuroshio current, tidal current and the bathymetry of the East China Sea Shelf. There may be many other phenomena whose behaviors have not been investigated by ship measurements, partially because one does not know what else oceanic phenomena near Taiwan have significance for research, and partially because of their transient or small scale nature such that one does not know where to look for them if they exist.

Repeated satellite visible and infrared observations may provide answers to some of the unresolved oceanic questions and problems. Thermal images from NOAA satellites indicate that there are thermal fronts, eddies, mushroom-like and filament structures in the sea northeast of Taiwan. But these observations are vulnerable to cloudiness, which unfortunately is quite persistent around Taiwan. Such cloudiness hinders the acquisition of sea surface temperature (SST) field and therefore the monitoring of oceanic responses to the change weather and marine environment. Moreover, interpretation of the NOAA IR images sometimes presents difficulties because of the high values and high variability of the total water vapor content in the atmosphere. The satellite passive microwave and scatterometer measurements of the sea surface temperature and wind speed (surface roughness) can be obtained at cloudy conditions, but they are not suitable for detailed oceanographic studies due to their poor spatial resolution. Real Aperture Radar (RAR) and Synthetic Aperture Radar (SAR) can also image the sea surface roughness through clouds because they operate in microwave frequencies, but with much finer spatial resolution: 1-3 km for RAR and 10-30 m for SAR. Although the surface roughness is mainly determined by surface wind, at low and medium wind speed, it also depends on the surface current and the surfactant concentration.

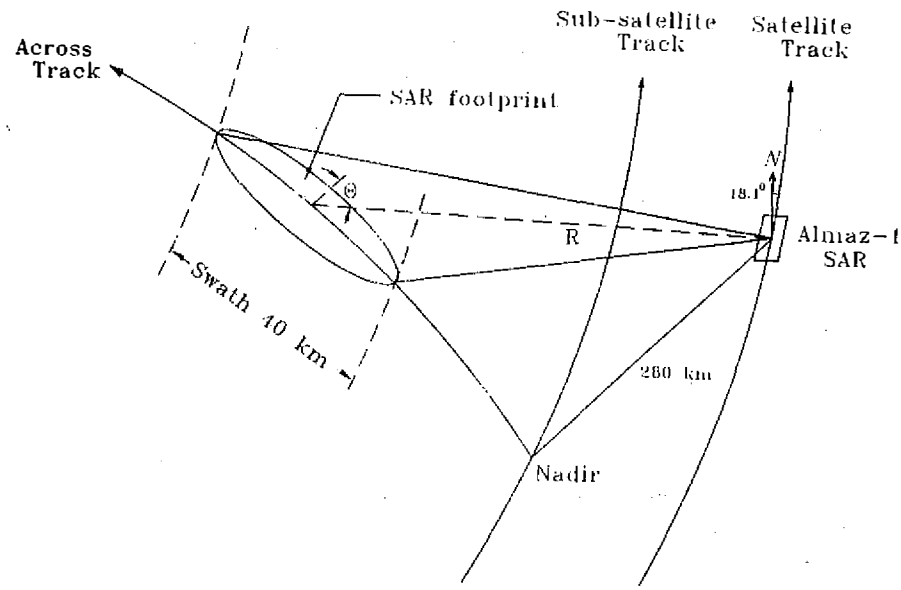

Fig. 1. The geometry of Synthetic Aperture Radar (SAR) imaging of earth surface, flight direction of Almaz-1 and direction of illumination.

In the following, the authors use the Russian Almaz satellite SAR images taken on 16 July, 1992 over the ocean northeast of Taiwan to exemplify the abundance of oceanic phenomena in this area. An attempt is made to explain the features of the distribution of brightness on these images as surface manifestations of internal waves, current, bottom topography and also as spatial wind variations and the presence of slicks. The NOAA IR images, weather maps and ship data taken almost simultaneously with the SAR image as well as bathymetric and nautical charts are used to interpret the signatures in the image of the SAR backscatter. Suggestions on the meteorological conditions and timing are presented for future dedicated expeditions for studying specific oceanographic phenomena northeast of Taiwan.

2. THE SYNTHETIC APERTURE RADAR (SAR)

The SAR transmits long chirp pulses (pulses with frequency changes linearly with time) to the sea surface and records returned echoes that are principally caused by resonant Bragg scattering from the sea surface. At the incidence angles θ (Figure 1) from 20° to 70°, the pulses with wavelength λ are scattered by the surface gravity-capillary and short gravity waves with a wavelength of $\Lambda=\lambda/(2 \sin \theta)$ projected in the radar range direction.

The slant range R between the satellite and the footprint (field of view of SAR) is determined by the time lapse from transmitting a pulse to receiving surface echoes. An ellipse may be formed by all the points on the earth surface having the same R. Other than the azimuthal symmetry, the Doppler shifts of echoes depend on the rate of change of R and therefore are all different. The source of returned echoes may thus be determined by their arrival time and frequency shift.

The ground resolution in the range direction, Δr, is determined by the relationship $\Delta r = c\tau/(2 \sin \theta)$, where τ is the effective (after compression) pulse width and c is the light speed. The ground resolution in the azimuthal (along-track) direction, $\Delta a = D/2$ (where D is the size of the antenna) is independent of the altitude of the satellite and the slant range of target. This is why SAR may have a ground resolution of the order of 10 meters *vs.* 10 km or more for the majority of satellite microwave sensors, except the RAR. A comprehensive description of the principles of SAR is given by Skolnik (1990) and Stewart (1985).

The Russian Almaz-1 satellite (1991-1992), like the Kosmos-1870 (1987-1989), was equipped with high-resolution imaging radar (Etkin *et al.*, 1994; Salganik *et al.*, 1990; Neronsky *et al.*, 1993). Table 1 lists the general parameters for the Almaz-1 SAR system and the SAR image of 16 July 1992, which will be discussed in this paper, was taken at an incidence angle of 35.9° with a swath width of 43 km. This means the intensity of backscattered signals is determined by surface waves with wavelengths Λ of 14~5 cm for θ in the range of 20° to 65°; at $\theta = 35.9°$, $\Lambda \approx 8$ cm. Such a small scale roughness (mainly ripples) would respond to the local wind change in seconds, implying that the gravity-capillary waves have very short memory by coming and going with the surface wind. Therefore, the analysis of the SAR and RAR imageries may reveal a complicated structure of the surface wind field (Gerling, 1986; Fu and Holt, 1982; Johannessen *et al.*, 1991; Mitnik, 1993).

In addition to wind, the modulation of surface roughness (intensity of backscattered signals) may be induced by long gravity waves, swell, divergence of surface currents in the areas of frontal boundaries, eddies, internal waves, upwelling, the variations of SST and surfactant, and the bottom topography (Beal *et al.*, 1981; Chelomei *et al.*, 1990; Ermakov *et*

al., 1992; Fu and Holt, 1982; Johannessen *et al.*, 1991; Mitnik and Lobanov, 1991; Veseky and Stewart, 1982; Wu, 1989). A number of factors (for example, the change of the SST and the surfactant concentration) can act simultaneously and influence the ripple spectrum in either direction. However, this modulation reveals interesting oceanic features only for the limited range of wind speed of about 1 m/s to 8 m/s.

Table 1. Almaz-1 SAR system parameters.

Height of orbit, km	300-370
Inclination, degree	73
Frequency, GHz	3.1
Wavelength, cm	9.6
Antenna size (along track x cross track), m	15 x 1.5
Beamwidth, degree	0.4 x 4
Polarization (transmission, reception)	HH
Mean incidence angle, degree	20 - 65
Slant range resolution, m	13 - 19
Azimuth resolution, m	13
Swath width (30 - 45), km	30 - 45

From the above, the interpretation of SAR images is clearly a complicated problem, especially at low and medium wind speeds when the variations of the sea roughness are caused by both the atmospheric and oceanic processes. The satellite observations of other spectral bands, surface weather and wave analysis maps, *in situ* data and knowledge of the region under investigation should be used to enhance the reliability of SAR image interpretation.

3. ENVIRONMENTAL CONDITIONS

From the weather map (surface analysis map) of 18:00 GMT July 16, 1992, prepared by the Central Weather Bureau on Taiwan, an approximate 2-7 m/s south wind was observed northeast of Taiwan (Figure 2). Both the R/V Akademik Aleksandr Vinogradov which was at (24°44'N, 122°33'E) and the Pengchiayu weather station reported a northward wind speed of 7-8 m/s around 20~21 GMT July 16, 1992. In accordance with the wave analysis map prepared by the Japan Meteorological Agency (JMA), wind waves of about 1.5 m of significant wave height and 5-second period propagated to the northeast (Figure 3). The variations of the sea surface temperature northeast of Taiwan determined by analyzing the NOAA-11 IR images of 06:54 GMT July 14, 19:08 GMT July 15 and 23:19 GMT July 19 were in the range of 27 to 29°. Patches and stretched northward and northeastward features of colder water were observed east of the SAR image, bordering the warmer Kuroshio water.

4. SOME OCEANIC PHENOMENA REVEALED IN THE SAR IMAGE

The radar image essentially represents a map of the ocean surface radar reflectivity. The brightness of the radar image increases with the backscattering signal level (sea surface roughness). A wealth of details in a structure of the brightness field is seen on the fragment of the SAR images covering the study area (Figure 4). This image fragment is about 23 km in width and about 130 km in length. To help locate the features, a grid is overlaid on the

image, with A-S denoting the northward direction and 1-5 the eastward direction. Pengchiayu Island is in grid K2, Mienhuayu Island in I3-I4 and Huapingyu Island in J1. Cape Pitou and Cape Santiao are in C2 and A5, respectively.

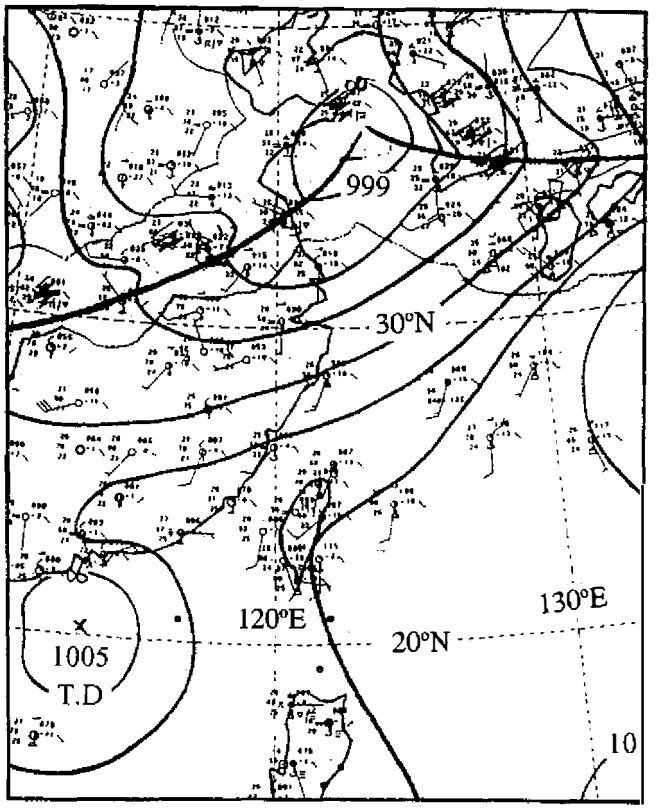

Fig. 2. The weather map (surface analysis map) of 18:00 GMT July 16, 1992 prepared by the Central Weather Bureau. Northward wind speed of 2-7 m/s was observed northeast of Taiwan.

The joint analyses of the outlines of the contrast features on the images, the bathymetric chart (Figure 5), the NOAA IR images, the atmospheric (winds, pressure field) and oceanic (waves, tides, currents) conditions and the ship measurements enable the researcher to suggest that most of the features are caused by the dynamic processes in the ocean and by the change in the physico-biological properties of the surface water influencing the surface roughness. The array of white lines near the western edge of this SAR image is not a natural phenomenon but an artifact of data processing. We shall exemplify the oceanic features (Figure 6) by their brightness patterns in the SAR images:

4.1 Slicks

Slicks are identified as smoothened (compared to surrounding regions) regions of the water surface. The smoothing is due to the decrease of small scale roughness (Fedorov and Ginsburg, 1988). This can be either a perfectly smooth region against the background of light ripples or a region with light ripples against the background of sharper gravity-capillary

waves. Slicks may appear as irregular patches, organized periodic structures and quasi-periodic ones. The occurrence of the slicks may be caused by damping action of surfactants or by dynamic factors of the subsurface layer, such as turbulence, current, convection, and internal waves. For example, regions with high concentration of plankton (like in upwelling regions) will be covered by surface films. If bilge water is dumped from a ship, it may spread out and form a thin artificial film over a patch or long filaments (generated by the shear of ocean current). However, slicks appear most often from a compromise between the surface wind distribution and factors mentioned above (Fedorov and Ginsburg, 1988). The slick areas are characterized by low radar backscattering and have dark tone on SAR image.

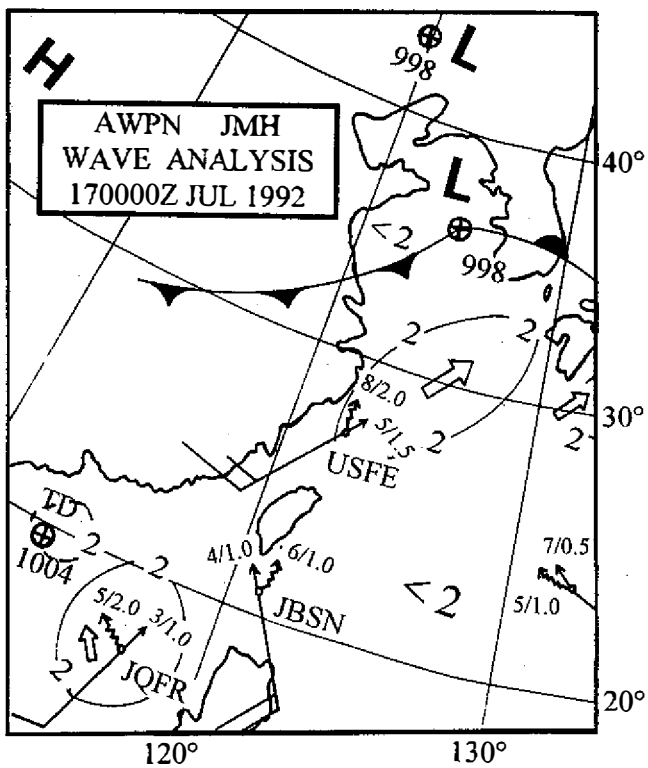

Fig. 3. The wave analysis map of 00:00 GMT July 17, 1992 prepared by the Japan Meteorological Agency. Wind waves about 1.5 m significant wave height and 5 seconds period propagated to the northeast.

A narrow dark band (slick area) G2-G5 of length about 15 km and width 0.5-1 km is just located in the upwelling region where cold waters were observed on NOAA IR images (Lin *et al.*, 1992) and from ship measurements (Liu *et al.*, 1992b). The position of the band coincides with a narrow east-west directed Huaping Canyon (Figure 5) that is a continuation of Mienhua Canyon (Song and Chen, 1992). This "coincidence" suggests that the formation of such slicks might be resulted from upwelling process because the generation of ripples and short gravity waves is lowered in upwelling areas (especially in large ones) by increased concentration of surface films and sometimes by a more stable marine atmospheric boundary

layer. The dissipation rate of these short waves also gets higher than in the surrounding water, partially due to surface divergence and turbulence associated with upwelling, and partially due to the increase of the bulk viscosity of water with the increase of surfactant concentration and the decrease of temperature. The last factor can give a significant contribution to the change of radar contrasts at large SST differences (Mitnik and Lobanov, 1991). Once water leaves the upwelling center, the turbulence dies down, the stability of surface air boundary weakens, the surfactant concentration and surface current decrease.

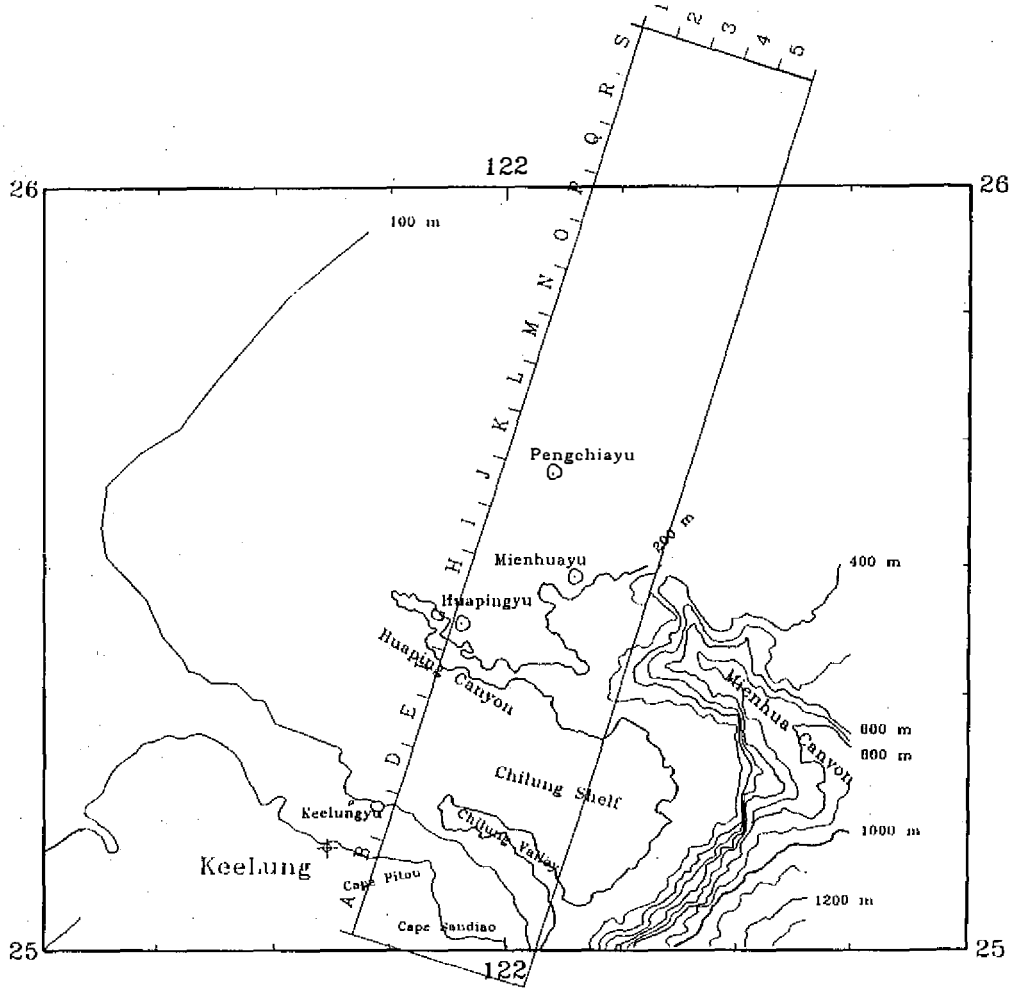

Fig. 5. The geographic location and bathymetry for SAR images in Figure 4.

It is possible, however, that a slick is not related to upwelling, but being antropogenic (pollution) or natural (for example, due to active seafloor oil and gas seepage (MacDonald *et al.*, 1993). Recent measurements have shown increased methane concentration in bottom waters northeast of Taiwan (Objirov, 1994). Nevertheless, the slick in G2-G5 is unlikely to be antropogenic, unless the pollutant had been dumped along the Canyon, an almost impossible case.

Major dark patches are in D2-E2 and in B3-C3. The decreased level of radar backscattering of these two regions could be either due to low wind speed at the lee of coastal mountains in B1-B2 and at 20 km southwest of D1, or due to increased surface film concentration. Damping of small scale roughness increases sharply when the surface films concentration exceeds a distinct threshold (Ermakov *et al.*, 1992; Monin and Krasitsky, 1985), while weak wind favors the damping.

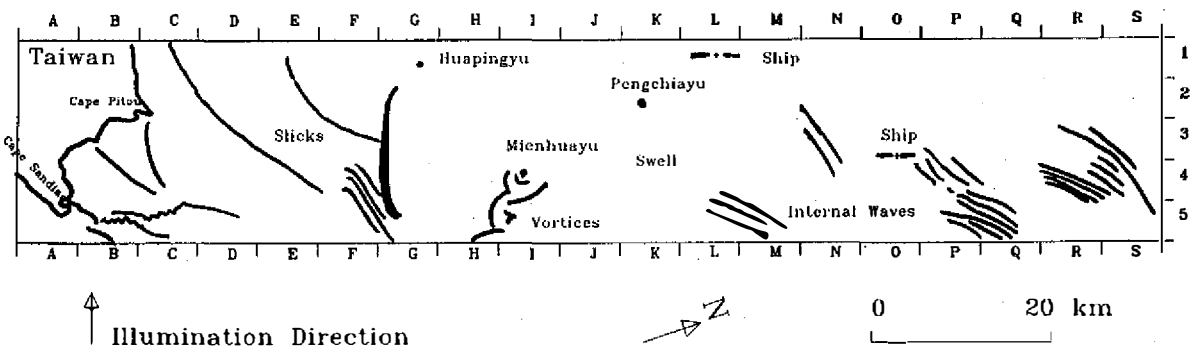

Fig. 6. Hand drawings of oceanic features redrawn from Figure 4.

4.2 Surface Waves

For deep water waves, the relation between wave period T (in sec.) and wavelength Λ (in meter) is approximately $\Lambda = 1.56\ T^2$. In the region east of Pengchiayu, namely K3-K5, the wavelength of swell is estimated to be 80 m to 250 m. This is equivalent to a wave period of 7 second to 12.7 second. Where did these swell come from?

One ship (call sign USFE for radio communication) reported 8 sec swell of 2 m height at about 150 km north of Pengchiayu (Figure 3). Because this swell propagated northward under southeasterly wind, it should be generated by a distant weather system, rather than by local wind. In the weather map of 00:00 GMT July 14, broadcasted by JMA, there was a tropical depression northeast of Mindanao, centered at (11°N, 129°E). A ship located about 300 km north of the depression center, reported 10 m/s wind. Within 100 km fetch distance, this 10 m/s wind could generate mature 8 sec wave of over 2 m wave height. Its wave length was about 100 m and group velocity was about 6.2 m/s, or 540 km/day. This wave could propagate to Pengchiayu (about 1700 km from the center of depression) by the time of Almaz-1 pass 7519 at 20:17 GMT of July 16.

In the same wave analysis map, 5 sec wind waves of 1.5 m wave height were also reported by the ship USFE. These waves were not visible on the SAR image because their wavelength is only about 40 m, close to the spatial resolution for visual analysis of Almaz-1 image. The theoretical size of Almaz-1 SAR footprint is 15 m at the near field (i.e. at the eastern edge of the image in Figure 4, close to the sub-satellite track), and 10 m at the far field (not shown in Figure 4 because of low signal-to-noise ratio). Therefore, waves with wavelength shorter than 30 m will be aliased into longer wave, and those with wavelength slightly larger than 30 m will have a reduced spectral power and suffer contamination from noise (speckles).

4.3 Internal Waves (IWs)

The bands of the alternating brightness (bands of rough and smooth sea surface) G5-F3 cross the eastern part of the slick area G2-G5. These bands comprise packet of internal wave fronts. These waves are frequently observed in stratified waters on the continental shelf. The main cause of IW generation in the coastal zones is the interaction between tidal current and the abrupt rising of the sea floor near continental shelf break, sills, etc. The wave fronts more or less repeat the typical features of isobaths and sometimes have a length of tens and hundreds of kilometers. When these waves travel over a shoaling bottom with progressively decreasing water depth, they become asymmetrical, ultimately break and produce intense mixing, which may have important effects on biological primary production (Haury *et al.*, 1979). Besides, these internal waves, with diurnal or semidiurnal frequencies, contribute to transport of planktonic larvae and suspended sediment in coastal waters (Boczar-Karakiewicz *et al.*, 1991; Pineda, 1991).

At wind speed below 7 m/s surface signatures accompany the underlying quasi-periodic oscillations. The IWs affect the whole wind wave spectrum and, therefore, the reflection and emission properties of the sea surface. Alternating bands of rough and smooth sea surface (the surface manifestations of the IW) were observed by the SAR, RAR, microwave radiometers and by optical cameras in many coastal regions and in the open ocean. Correlation between the surface signatures and the IW was investigated by many authors (Apel and Gonzales, 1983; Fu and Holt, 1982; Liu, 1988; Shuchman *et al.*, 1988). In many cases, their energy is sufficient to modulate the small scale surface roughness significantly as a result of either or both of two mechanisms: (1) film mechanism (redistribution of the surfactant concentration with higher damping of ripples in the surface water convergence zones) and (2) kinematics mechanism (a periodic modulation of ripples' height by their interaction with the IW-induced surface currents).

Almaz-1 SAR sensing was performed two days after full moon when tidal current intensity is close to its maximum. The SAR image showed that the IW wavelength in the group G5-F3 changes from about 1 km to 0.5-0.6 km that points to the nonlinear process (Apel and Gonzales, 1983; Osborne and Burch, 1980; Liu, 1988). The length of IW crests is more than 10-15 km (Probably, the Almaz-1 SAR registered the western part of this packet only.) The interaction of tidal current with abrupt depth change at the eastern edge of Chilung Shelf is a probable source of the IW generation: the orientation of isobaths in the area 25°00'-25°10'N and 122°10'-122°20'E (about 35-40 km east of IW packet) is nearly parallel to IW crests. The stratification of density, derived from hydrographic measurements of R/V Vinogradov in this region for 15-17 July 1992, was favorable for the IW generation.

Signatures of IW with different wavelengths, orientation and intensity are seen on the SAR image north of Pengchiayu island. The probable cause of IW generation is the sharp change of bathymetry near shelf break and the sea mounts east of Mienhuayu island. As IW packet propagates outward from the source region, its wave fronts assume concave shape (just like surface gravity waves emanating from the source) and the distance between successive wave fronts decreases toward the rear, or the source region. In the northern most IW packet in S5-R3 that propagated in NNW direction, the first IW front is clearer and larger than the others. The wavelength changes here from 700 m to 500 m.

The radar contrasts of a packet Q5-P3 are higher than that for the IW packet in S5-R3, and they are aligned to each other. This indicates that the Q5-P3 packet was generated one semidiurnal (12.4 hr) tidal cycle later than the S5-R3 packet. The inter packet separation

determined from the SAR image is about 13 km and the corresponding nonlinear group speed is about 0.3 m/s, which is typical for the propagation of IWs (Apel and Gonzales, 1983). The distance between the first two dark bands on the northwestern edge of Q5-P3 packet is about 1200 m while the trailing waves are near 500 m. The distortion of the bands in area Q5 is, probably, associated with local variation of surface current (Ochadlick *et al.*, 1992).

Four bands in R4 (Figure 4 & 5) located south of the packet in S5-R3 have the wavelength of about 500 m and propagated in WNW direction. The internal waves in N3-N4 and in M5-L4 have wavelength about 1 km.

4.4 Bottom Topography and Current Features

Two curved white bands emanating from Cape Pitou to C3 and to C3-C4, a group of bands with different brightness and orientation in A5-B5 off Cape Santiao, two wavy filaments in B5-C5, the bright patch in C4, etc., all indicate higher surface roughness. Some of them are also co-located with area of the rip current marked on nautical charts (Chinese Navy Chart No. 0360 and 0350). Coastal flood current of 0.5-1.0 m/s off Cape Santiao and Cape Pitou and southeastward ebb current of 0.5-1.5 m/s farther off Cape Santiao are also shown on these charts. An interaction of the spatially-inhomogeneous currents with a system of the relatively small submarine ridges and valleys, the large Chilung Valley, Cape Pitou and Cape Santiao and with wind waves can cause modulation of lengths and amplitudes of the surface waves, their large-scale bending, and result wave convergence and divergence zones in this region. From above considerations it follows that SAR registered a typical distribution of surface roughness corresponding to definite phase of tide in the region under study.

Two wavy filaments in B5-C5 reflect some quasi-periodic process with wavelength about 1 km and amplitude 200-300 m. It may be suggested that they were generated by the interaction between near-shore flow and obstacles off Cape Santiao. In this case the rough waters down stream from a sea mount is similar to ship wakes. At first, they form straight narrow bands of increased roughness and then wave-like filaments. The western filament (about 100 m wide) is better visible than the eastern one, because it has larger radar contrast against the dark band in C5 east of it.

4.5 Vortices Downstream of an Island

Probably, the bathymetric related signatures of the ocean surface can be seen also in Figure 4 around Pengchiayu and Mienhuayu islands. When this SAR image was taken (20:17 GMT of July 16), the Keelung sea level was at its minimal height, 1.10 m, between 20:00 - 22:00 GMT. The tidal current over East China Sea should be near the end of southeastward ebb tide. Curved bright bands and patches in I4-I5 should be generated by an obstacle (Mienhuayu island) amid this strong southeastward ebb current. This kind of vortex-shedding from a small obstacle are often seen in the island wakes (Pattiaratchi *et al.*, 1986; Davis and Mofor, 1990) and the cloud pattern behind mountainous islands, in particular, behind Cheju Island (33°N, 126°E) during cold air outbreaks. Lack of detailed current measurement and bathymetric charts prevents further comparison.

4.6 Ships and Ship Tracks

A pair of small bow wakes (white lines) in P4 shows the track of a south-bound ship. Another pair of bow wake and stern wake (dark line) of southeast-bound ship can be seen

in P3-O5. The more visible patterns are bright points in O3 and L1 show positions of ships. Dark and light lines emanating from a point in O3 along the direction of satellite track are related to the interference pattern of SAR antenna.

5. DISCUSSION AND CONCLUSION

Satellite observations of different properties of the sea surface, especially the surface roughness, offer means for monitoring oceanic phenomena and processes. For regions of high cloudiness (such as near Taiwan), the capability of SAR to monitor the spatial variability of ocean circulation, sea surface properties and the wind structure, in spite of cloudiness and sun illumination (day or night) is of particular importance. Their temporal variability can also be monitored and studied after the launch of European ERS-2 satellite at the end of 1994, Canadian Radarsat in February of 1995, and Japanese ADEOS satellite in 1996. The wind limitations, however, mean that the SAR gives an "all-weather" capability only for some applications. This is not true for all studies of oceanic phenomena (Gower *et al.*, 1993).

In this paper, the features of the brightness distribution on Almaz-1 SAR image of pass 7519 are discussed. To our knowledge, it is the first analysis of the SAR image covering waters near Taiwan. These features are due to the surface small scale roughness modulation resulted from both the atmospheric and oceanic processes.

Several of these features were reliably interpreted as related to irregularities in the relief of sea bed. Lack of detailed bathymetric charts and data about currents prevents their exact correlation with signatures on the surface. However, the results of similar investigations for other regions (Fu and Holt, 1982; Hennings *et al.*, 1993, Shuchman, 1982; Schuchman *et al.*, 1985; Vogelzang *et al.*, 1991) have demonstrated the possibilities of the mapping of shallow water bottom topography with imaging radar. According to theoretical analysis and laboratory experiments (Long *et al.*, 1993), formation of radar signatures is associated with tidal current spatial variations that are caused by bathymetric features. In turn, zones of strong current gradient can trap wave energy, which will shift the wave number into gravity-capillary region and produce the increased backscattering. Regular receiving of ERS-1 SAR images over coastal waters of Taiwan will allow us to watch the bottom irregularities and, in particular, the changing of location and form of sand bars in Taiwan Strait and in other regions. Since observational evidence to support the above mentioned theoretical results is still rare, arrangement of special sea expedition should be considered as a priority task.

Interpretation of quasi-periodic structures with wavelengths of several hundred meters as surface expression of IW is also beyond any doubt. Measurements of simple characteristics of IW packets such as interpacket separation, variation of wavelengths within a given packet, the curvature of the packet isophase fronts in conjunction with a simple hydrodynamic model (Apel and Gonzales, 1983) offer means for determining wave amplitude and degree of nonlinearity. Peculiarities of nonlinear IW northeast of Taiwan became the subject of investigation by Liu and Mickett (1994). Using the ERS-1 SAR images taken in autumn 1992 and the hydrographic data, they have identified internal waves of elevation (as opposite to usually observed IW of depression where the surface mixed layer thickens and the thermocline deepens at the IW front) due to a thicker mixed layer as compared with the bottom layer on the continental shelf. They also suggested to take into account the influence of the Kuroshio for generation of IW. So far, the IW has not been studied in detail by local oceanographers.

Reliable interpretation of slicks is a difficult problem too. Systems of quasi-periodic dark bands (slicks) are definitely due to IW. But it is impossible to estimate a relative contribution of the surfactants and variable currents in their formation. Dark patches and bands may reflect the features of distribution both of wind stress (Mitnik, 1993) and surfactants such as natural or spilled oil. Collection and analysis of chemical and physical properties of slick samples are essential in the development of scientific and practical problem including oil pollution monitoring.

Recently, we obtained several ERS-1 SAR images taken over waters surrounding Taiwan. These images were received and processed at National Central University. The images for November 10 and 15, 1993 (14 November was a new moon) partially overlap with the Almaz-1 SAR image and show distinctly the topographically induced features east of Cape Pitou and Cape Santiao, the internal wave packets propagating both shoreward and seaward, several slicks on Chilung Shelf, and also features of the brightness distribution associated with wind action. In particular, IW had wave crests of 50 km and more, and the nonlinear group speed for packets propagating in both directions was about 0.35 m/s. We have started digital analysis of these images to interprete them with tidal observations and IW model.

In such a manner, earlier research and our analysis have demonstrated the potential of SAR for studying the ocean dynamics (currents, eddies, fronts, etc.) and the air-sea interaction, for improving nautical charts, and for monitoring the changing coastline and water pollution. In connection with this, arranging expeditions at northeast of Taiwan for a detailed study of revealed anomalies is required. To have reliable in situ data for comparison with satellite SAR images, ship measurements should be carried out at certain conditions. In particular, to study the visibility of bottom topography features in SAR imagery, current must be at least 0.4 m/s and a wind of at least 1 m/s, but not greater than 8 m/s, with at least some component in the range direction (Shuchman *et al.*, 1982). The research vessel should be equipped with Acoustic Doppler Current Profiler, echo sounder, Global Positioning System receiver, hydrophysical probes, and anemometer. The sharp change of surface roughness can be registered by a marine radar and microwave radiometers operating at centimeter and millimeter wavelengths. A series of field work is underway to study the cause of bright and dark bands and patches in SAR images that are associated with bathymetry and IW.

Acknowledgments This research was sponsored by the Council of Agriculture through research grant 83-RS-04-02, and by the National Science Council through research grants NSC-82-0209-M002a-046W, NSC-83-0209-M019-010 and NSC-83-0102-C019-004-SM. We greatly appreciate anonymous reviewers' thoughtful commnets on improving this paper.

REFERENCES

Apel, J. R., and F. I. Gonzales, 1983: Non-linear features of internal waves of Baja California as observed from the Seasat imaging radar. *J. Geophys. Res.*, **88**, 4459-4466.

Beal, R. C., P. S. DeLeonibus, and I. Katz (Eds.), 1981: Spaceborne Synthetic Aperture Radar for Oceanography. Johns Hopkins University Press, Baltimore, Md., 216pp.

Boczar-Karakiewicz, B., J. L. Bona, and B. Pelchat, 1991; Interaction of internal waves with the seabed on continental shelves. *Contin. Shelf Res.*, **11**, 1181-1197.

Chelomei, V. N., G. A. Efremov, K. T. Litovchenko, L. B. Neronskii, P. O. Salganik, S. S. Semenov, A. V. Smirnov, and V. S. Etkin, 1990: High-resolution radar sensing of the sea surface from "Kosmos-1870" satellite. *Issledovanie Zemli iz Kosmosa*, **N2**, 80-90 (in Russian).

Davies, P. A., and L. A. Mofor, 1990: Observation of flow separation by an isolated island. *Int. J. Remote Sensing*, **11**, 767-782

Ermakov, S. A., S. G. Salashin, and A. R. Panchenko, 1992: Film slicks on the sea surface and some mechanisms of their formation. *Dynam. Atmos. Oceans*, **16**, 279-304.

Etkin, V., K. Litovchenko, S. Semenov, P. Shirokov, and A. Ivanov, 1994: SAR imaging of the ocean: New results obtained by Almaz-1 satellite. Proc. of the Pacific Ocean Remote Sensing Conference, Melbourne, Australia, 1-4 March 1994, 399-407.

Fedorov, K. N., and A. I. Ginsburg, 1988: The Subsurface Layer of the Ocean. Hydrometeoizdat, Leningrad, 304pp (in Russian).

Fu, L.-L., and B. M. Holt, 1982: Seasat views oceans and sea ice with Synthetic-Aperture Radar. NASA/JPL Publication 81-120, 200pp.

Gerling, T. W., 1986: Structure of the surface wind field from the Seasat SAR. *J. Geophys. Res.*, **91**, 2308-2320.

Gower, J. F. R, P. W. Vachon, and H. Edel, 1993: Ocean applications of RADARSAT. *Canadian J. Remote Sensing*, **19**, 372-383.

Haury, L. R., M. G. Briscoe, and M. H. Orr, 1979: Tidally generated internal wave packets in Massachusetts Bay. *Nature*, **278**, 312-317.

Hennings, I., H. Pasenau, and F. Werner, 1993: Sea surface signatures related to subaqueous dunes detected by acoustic and radar sensors, *Contin. Shelf Res.*, **13**, 1023-1043.

Hsueh, Y., J. Wang, and C.-S. Chern, 1992: The intrusion of the Kuroshio across the continental shelf northeast of Taiwan. *J. Geophys. Res.*, **97**, 14323-14330.

Johannessen, J. A., R. A. Schuchman, O. L. Johannessen, K. L. Davidson, and D. R. Lyzenga, 1991: Synthetic aperture radar imaging of upper ocean circulation features and wind fronts. *J. Geophys. Res.*, **96**, 10411-10422.

Lin, C.-Y., C.-Z. Shyu, and W.-H. Shih, 1992: The Kuroshio fronts and cold eddies off northeastern Taiwan observed by NOAA-AVHRR imageries. *TAO.*, **3**, 225-242.

Liu, A. K. 1988: Analysis of nonlinear internal waves in the New York Bight. *J. Geophys. Res.*, **93**, 12317-12329.

Liu, A. K. and Mickett, 1994: Nonlinear internal waves observed northeast of Taiwan by ERS-1 SAR. Proc. of the Pacific Ocean Remote Sensing Conference, Melbourne, Australia, 1-4 March 1994, p.409.

Liu, C.-T. 1983: As the Kuroshio turns: (I) characteristics of the current. *Acta Oceanogr. Taiwanica*, **14**, 88-95.

Liu, C.-T., and S.-C. Pai, 1987: As Kuroshio turns: (II) The oceanic fronts north of Taiwan. *Acta Oceanogr. Taiwanica*, **18**, 49-61.

Liu, K.-K., G.-C. Gong, C.-Z. Shyu, S.-C. Pai, C.-L. Wei and S.-Y. Chao, 1992a: Response of Kuroshio upwelling to the onset of northeast monsoon in the sea north of Taiwan: Observations and a numerical simulation. *J. Geophys. Res.*, **97**, 12511-12526.

Liu, K.-K., G.-C. Gong, S. Lin, C.-Y. Yang, C.-L. Wei, S.-C. Pai, and C.-K. Wu, 1992b: The year-round upwelling at the shelf break near the northern tip of Taiwan as evidenced by chemical hydrography. *TAO.*, **3**, 243-275.

Long, S. R., R. J. Lai, Huang N. E., and G. R. Spedding, 1993: Blocking and trapping of waves in an inhomogeneous flow. *Dynam. Atmos. Oceans*, **20**, 79-106.

MacDonald, I. R., N. L. Guinasso, Jr., S. G. Ackleson, J. F. Amos, R. Duckworth, R. Sassen, and J. M. Brooks, 1993: Natural oil seepage in the Gulf of Mexico visible from space. *J. Geophys. Res.*, **98**, 16351-16364.

Mitnik, L.M. and V.B. Lobanov, 1991: Reflection of the oceanic fronts on the satellite radar images. In: K. Takano, (Ed.), Oceanography of Asian Marginal Seas, Elsevier Oceanography Series, 54, Elsevier, Amsterdam, 85-101.

Mitnik, L. M., 1993: Surface wind variability from the Satellite Side Looking radar. In: I. S. F. Jones, Y. Sugimory and R. W. Stewart (Eds.), Satellite Remote Sensing of the Oceanic Environment, Seibutsu Kenkyusha, 200-208.

Mitnik, M. L., C. T. Liu, and L. M. Mitnik, 1994: Analysis of concurrent subsurface water temperature and stimulated fluorescence measurements in the East China Sea. Paper presented at the Fifth KEEP-WOCE Conference, 214-225.

Monin, A. S., and V. P. Krasitsky, 1985: Phenomena on the Ocean Surface. Hydrometeoizdat, Leningrad, 375pp (in Russian).

Neronsky, L. B., V. G. Kobernichenko, and S. M. Zraenko, 1993: Digital formation of the earth surface radar images in the "Almaz-1" space apparatus SAR. *Issledovanie Zemli iz Kosmosa*, **N4**, 33-43 (in Russian).

Objirov, A. I., 1994: Dissolved gas distribution in sea water columns off northeastern Taiwan. Proceeding of The Fifth KEEP and WOCE Conference, 2-5, Feb. 1994, Chiayi, Taiwan, ROC.

Ochadlick, A. R., P. Cho, and J. Evans-Morgis, 1992: Synthetic aperture radar observations of current colocated with slicks. *J. Geophys. Res.*, **97**, 5325-5330.

Osborn, A. R., and T. L. Burch, 1980: Internal solitons in the Andaman Sea. *Science*, **208**, 451-460.

Pattiaratchi, C., A. James, and M. Collins, 1986: Island wakes and headlines eddies: a comparison between remotely-sensed data and laboratory experiments. *J. Geophys. Res.*, **92**, 783-794

Pineda, J., 1991: Predictable upwelling and the shoreward transport of planktonic larvae by internal tidal bores. *Science*, **253**, 548-551.

Salganik, P. O., G. A. Efremov, L. B. Neronskii, M. G. Kulikovskii, A. A. Kurmaev, V. I. Ivanyuk, and L. G. Tsifrinovich, 1990: Radar sensing of the Earth from "Kosmos-1870" satellite. *Issledovanie Zemli iz Kosmosa*, **N2**, 70-79 (in Russian).

Shuchman, R. A., 1982: Quantification of SAR signatures of shallow water ocean topography. Ph. D. Dissertation, The University of Michigan, 130pp.

Shuchman, R. A., D. R. Lyzenga, and G. A. Medows, 1985: Synthetic aperture radar imaging of ocean-bottom topography via tidal-current interactions: theory and observations. *Int. J. Remote Sensing*, **6**, 1179-1200.

Shuchman, R. A., D. R. Lyzenga, B. M. Lake, B. A. Hughes, R. F. Gasparovich, and E. S. Kasishke, 1988: Comparison of Joint Canada-U.S. Ocean Wave Investigation Project synthetic aperture radar data with internal wave observations and modeling result. *J. Geophys. Res.*, **93**, 12283-12291.

Skolnik, M. I. (Ed.), 1990: Radar Handbook, 2nd ed., McGraw-Hill, New York.

Stewart, R. H., 1985: Methods of Satellite Oceanography. Univ. of California Press, 360pp.

Song, G.-S., and M.-P. Chen, 1992: Bathymetry of KEEP area northeast of Tai-Wan, Institute of Oceanography, National Taiwan University.

Veseky, J. F., and R. H. Stewart, 1982: The observation of ocean surface phenomena using imagery from the Seasat synthetic aperture radar: An assessment. *J. Geophys. Res.*, **87**, 3397-3430.

Vogelzang, J., G. J. Wensink, I. Hennings, W. Alpers, J. P. Matthews, and D. Van Halesma, 1991: Mapping of sea bottom topography in a multi sensor approach: overview and preliminary results. Proc. IGARSS'91, Espoo, Finland, 2039-2041.

Wu, J., 1989: Suppression of oceanic ripples by surfactant-spectral effects deduced from sun-glitter, wave-staff and microwave measurements. *J. Phys. Oceanogr.*, **19**, 238-245.